Available online at www.sciencedirect.com
SCIENCE DIRECT®
Journal of Magnetic Resonance 173 (2005) 153–159
JMR Journal of Magnetic Resonance
www.elsevier.com/locate/jmr

A new approach for simultaneous measurement of ADC and T_2 from echoes generated via multiple coherence transfer pathways

Henry Ong[a], Chih-Liang Chin[a], Suzanne L. Wehrli[b], Xiaoping Tang[c], Felix W. Wehrli[a,*]

[a] *Laboratory for Structural NMR Imaging, Department of Radiology, University of Pennsylvania Medical Center, Philadelphia, PA, USA*
[b] *NMR Core Facility, Children's Hospital of Philadelphia, Philadelphia, PA, USA*
[c] *Department of Physics, University of Nevada at Reno, Reno, NV, USA*

Received 31 August 2004; revised 19 November 2004
Available online 21 January 2005

Abstract

The study of rotational and translational diffusion requires the measurement of both T_2 and apparent diffusion coefficient (ADC), quantities that are typically measured in separate experiments. The exploitation of echoes generated via multiple coherence transfer pathways offers an opportunity for measuring T_2 and ADC values simultaneously in a single experiment. A series of RF pulses can generate multiple echoes via different coherence pathways with each one being uniquely encoded. Here, we demonstrate one pulse sequence that uses an initial θ RF pulse to generate three coherence orders ($C = 0, -1, +1$). In the particular version of the method discussed here only two are used ($C = 0, +1$). Each order is encoded with a different b value from which the ADC is derived. The coherence order echo $C = 0$ is refocused to quantify T_2. The performance of the method—dubbed simultaneous measurement of ADC and relaxation time (SMART)—is demonstrated on a set of samples differing in T_2 and ADC achieved by varying the relative volume fractions in mixtures of gadolinium-doped H_2O and D_2O. The regional SMART derived T_2 and ADC agree well with those obtained with conventional double-spin–echo and pulsed gradient spin–echo methods.

Keywords: Multiple coherence pathways; Diffusion; T_2 relaxation; Multiple echoes; ADC

1. Introduction

Measurements of the apparent diffusion coefficient (ADC) in NMR for probing molecular displacements rely on the use of static or pulsed magnetic field gradients [1,2]. A major limitation for the study of diffusion in MR imaging is the long acquisition times necessary for accurate characterization of the ADC. The present work aims to improve ADC measurement efficiency and is an extension of the method proposed by Song and Tang [3]. Their multiple modulation multiple echoes (MMME, pronounced *M-M-Me*) NMR technique is similar to PREVIEW [4] and QUEST [5] and exploits echoes generated by multiple coherence transfer pathways. The magnetization generated in each coherence pathway has different diffusion weighting (characterized by a specific b value) so that echoes with multiple b values can be acquired simultaneously in one scan. Song and Tang successfully demonstrated their method with the measurement of the ADC of water.

Our work develops the MMME method into an imaging sequence. Here, we decided to start from a spin–echo sequence rather than a stimulated echo sequence as used by Song and Tang. Furthermore, this sequence was modified to include capabilities for the measurement of T_2 so as to allow simultaneous study of rotational and translational diffusion. NMR diffusion [6–8] and relaxation measurements [9–11] are important tools used to investigate the structure of porous media, such as oil well logging, micro-filtration, plant physiol-

* Corresponding author. Fax: +1 215 349 5925.
E-mail address: wehrlif@uphs.upenn.edu (F.W. Wehrli).

1090-7807/$ - see front matter © 2004 Elsevier Inc. All rights reserved.
doi:10.1016/j.jmr.2004.11.030

ogy, and biomedicine, and the correlation between the two are being studied [12,13].

In this paper, we will first discuss the pulse sequence designed for our method—dubbed simultaneous measurement of ADC and relaxation time (SMART). Several methods for combining relaxation and ADC measurements have previously been proposed [14,15]. van Dusschoten et al. [15] also proposed a technique that yields both ADC and T_2 from a single experiment, achieved by concatenating a pulsed gradient spin–echo (PGSE) and CPMG pulse sequence. Fundamentally different from this approach, the SMART method uses two coherence transfer pathways, as compared with just one. Each pathway is encoded with a different b value, and the signal from both is used to calculate the ADC value. The signal from one pathway is refocused to quantify T_2. ADC and T_2 measurements are not coupled by the nature of exploiting two coherence pathways and can be calculated independently.

The performance of the new method is demonstrated on two samples. The first sample contains 1 mM Gd-DPTA doped H_2O and the second sample contains five-compartments each with varying ADC and T_2 values. The SMART derived T_2 and ADC maps for the two phantoms are shown to agree well with those obtained with conventional double-spin–echo and PGSE methods.

2. Theory

2.1. Coherence pathways

The SMART technique is based the MMME method described by Song and Tang [3]. The theoretical basis for the MMME is extensively detailed in their paper and we will only summarize the relevant sections needed to understand the SMART method.

Let us define three states of spin magnetization for an ensemble of spin-1/2 nuclei as defined by Song and Tang [3]:

$$\begin{aligned} M_0 &= M_z, \\ M_+ &= \frac{M_x + \mathrm{i}M_y}{\sqrt{2}}, \\ M_- &= \frac{M_x - \mathrm{i}M_y}{\sqrt{2}}. \end{aligned} \tag{1}$$

These states are designated a coherence order C, which can be 0, +1, or −1 (or 0, +, −), respectively. A RF pulse rotates the magnetization vector, $\mathbf{M} \equiv (M_+, M_-, M_0)$, and therefore can change the coherence order M, depending on the coherence order before the RF pulse and the flip angle,

$$\mathbf{M}(t_\mathrm{p}) = \mathbf{R} \cdot \mathbf{M}t(0), \tag{2}$$

where $\mathbf{M}(t_\mathrm{p})$ and $\mathbf{M}(0)$ are the magnetization vectors before and after the pulse of duration t_p. In this paper, the rotation matrix $\mathbf{R}$ will only consider the on-resonance case. The RF flip angle is $\theta = \omega_1 t_\mathrm{p}$, where ω_1 is the Larmor frequency of the RF pulse. For the magnetization vector, $\mathbf{M} \equiv (M_+, M_-, M_0)$, the rotation matrix is

$$\mathbf{R}(\theta) = \begin{pmatrix} \frac{1+\cos\theta}{2} & \frac{1-\cos\theta}{2}\mathrm{e}^{\mathrm{i}2\phi} & -\mathrm{i}\frac{\sin\theta}{\sqrt{2}}\mathrm{e}^{\mathrm{i}\phi} \\ \frac{1-\cos\theta}{2}\mathrm{e}^{-\mathrm{i}2\phi} & \frac{1+\cos\theta}{2} & \mathrm{i}\frac{\sin\theta}{\sqrt{2}}\mathrm{e}^{-\mathrm{i}\phi} \\ -\mathrm{i}\frac{\sin\theta}{\sqrt{2}}\mathrm{e}^{-\mathrm{i}\phi} & \mathrm{i}\frac{\sin\theta}{\sqrt{2}}\mathrm{e}^{\mathrm{i}\phi} & \cos\theta \end{pmatrix}, \tag{3}$$

where ϕ is the phase of the RF pulse. An arbitrary pulse sequence will contain a train of N pulses. A coherence pathway is characterized by a series of $N+1$ coherence orders, $Q = (C_0, C_1, \ldots, C_N)$, where $C_0 = 0$ as all the magnetization will be along the longitudinal axis before the first pulse. The echo, E_Q, formed from a unique coherence pathway will depend on three factors: the pulse sequence, diffusion, and relaxation. Furthermore, if the timings between the RF pulses are unequal, then it is possible to separate different echoes arising from different coherence transfer pathways.

2.2. SMART sequence

The pulse sequence implemented in this paper is shown in Fig. 1A. The first θ RF pulse generates three states of spin magnetization (M_+, M_-, and M_0) each corresponding to the coherence orders $C = +1$, -1, and 0, respectively. Since we only need two coherence orders for our SMART method, we can use either $C = 0$, $+1$ or $C = 0$, -1. Here, we chose to use $C = 0$, $+1$, and since $C = +1$ is the distinguishing order, we call this pulse sequence SMART P. The echo formed by the coherence order $C = +1$ will be named the P echo. The echo formed by the coherence order $C = 0$ will be named the Z echo. The Z echo is refocused to form the Z2 echo. The coherence pathway for each echo is described below and a phase diagram is shown in Fig. 1B. The observable coherence order is defined as +1.

For the P echo, the coherence pathway is $Q = (0, +1, -1, \text{ and } +1)$:

$$\begin{aligned} M_0 &\xrightarrow{\theta_{\phi_1}} -\mathrm{i}\frac{\sin\theta}{\sqrt{2}}\mathrm{e}^{\mathrm{i}\phi_1}M_+ \xrightarrow{\pi/2_{\phi_2}} -\mathrm{i}\frac{\sin\theta}{2\sqrt{2}}\mathrm{e}^{\mathrm{i}(\phi_1-2\phi_2)}M_- \\ &\xrightarrow{\pi_{\phi_3}} -\mathrm{i}\frac{\sin\theta}{2\sqrt{2}}\mathrm{e}^{\mathrm{i}(\phi_1-2\phi_2+2\phi_3)}M_+. \end{aligned} \tag{4}$$

For the Z echo, the coherence pathway is $Q = (0, 0, -1, \text{ and } +1)$:

$$M_0 \xrightarrow{\theta_{\phi_1}} M_0\cos\theta \xrightarrow{\pi/2_{\phi_2}} \mathrm{i}\frac{\cos\theta}{\sqrt{2}}\mathrm{e}^{-\mathrm{i}\phi_2}M_- \xrightarrow{\pi_{\phi_3}} \mathrm{i}\frac{\cos\theta}{\sqrt{2}}\mathrm{e}^{\mathrm{i}(-\phi_2+2\phi_3)}M_+. \tag{5}$$

For the Z2 echo, the coherence pathway is $Q = (0, 0, +1, -1, \text{ and } +1)$:

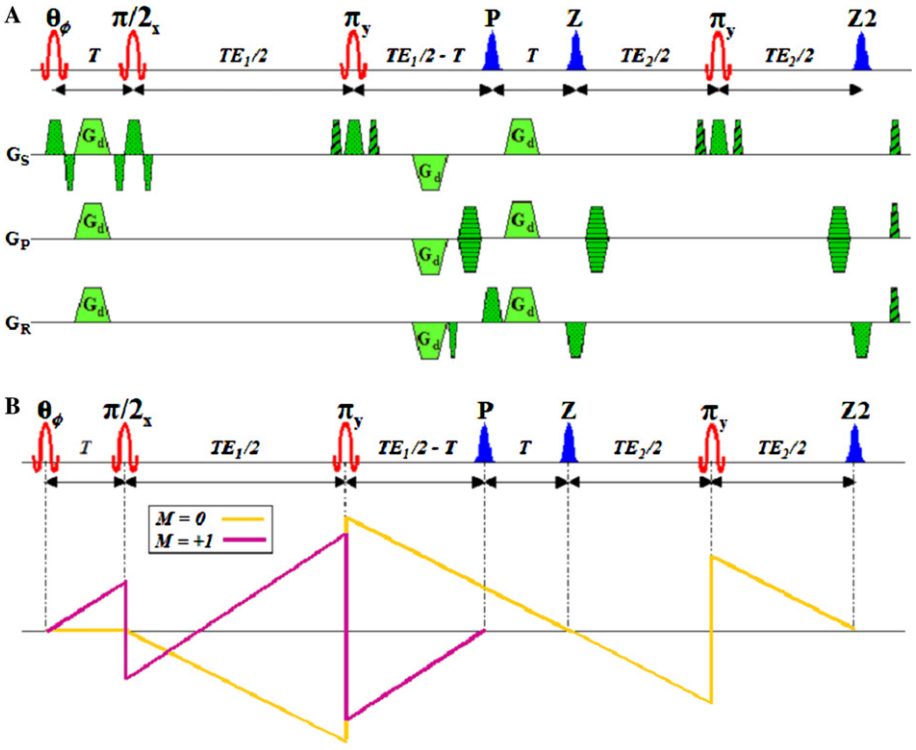

Fig. 1. (A) SMART P pulse sequence (not drawn to scale). Spoiling gradients were placed around the π pulses and at the end to prevent spurious echoes. (B) Phase diagram for SMART P pulse sequence (not drawn to scale).

$$M_0 \overset{\theta_{\phi_1}}{\rightarrow} M_0\cos\theta \overset{\pi/2_{\phi_2}}{\rightarrow} -\mathrm{i}\frac{\cos\theta}{\sqrt{2}}\mathrm{e}^{\mathrm{i}\phi_2}M_+ \overset{\pi_{\phi_3}}{\rightarrow} -\mathrm{i}\frac{\cos\theta}{\sqrt{2}}\mathrm{e}^{\mathrm{i}(\phi_2-2\phi_3)}M_- \overset{\pi_{\phi_4}}{\rightarrow} -\mathrm{i}\frac{\cos\theta}{\sqrt{2}}\mathrm{e}^{\mathrm{i}(\phi_2-2\phi_3+2\phi_4)}M_+. \quad (6)$$

The flip angle θ is chosen such each coherence order is of equal magnitude. The theoretical value of θ predicted is 63.4°. After the initial θ RF pulse a gradient G_d is applied. This gradient will only impart a spatial modulation on transverse magnetization. Therefore, the coherence order $C = +1$ will become spatially modulated while the coherence order $C = 0$ does not. A second gradient that is opposite in polarity in relation to the first one is applied after the π pulse and will act to rewind the spatial modulation of signal arising from the $C = +1$ coherence order while modulating the signal from the $C = 0$ coherence order. A third gradient that is now opposite in polarity relative to the second gradient is applied after the acquisition of the P echo and will rewind the modulation of the $C = 0$ signal. Due to diffusion, the second and third gradient pulses will not fully reverse the modulation of the first and second and the P and Z echoes will be attenuated accordingly. This attenuation can be described in terms of the echo intensity E

$$\ln\left(\frac{E(b_1)}{E(b_2)}\right) = -(b_1 - b_2)D, \quad (7)$$

where D is the self diffusion coefficient, and b is the b value which is defined for unrestricted diffusion as [2]

$$b = \gamma^2 \int_0^{TE} \left[\int_0^t \boldsymbol{G}(t')\mathrm{d}t'\right]^2 \mathrm{d}t, \quad (8)$$

where $\boldsymbol{G}(t) = [G_x, G_y, \text{and } G_z]$ is the analytical expression for the gradient–pulse sequence. To calculate the ADC, the amplitudes and the b values of the P and Z echoes are required. The calculations of the b values were done with a numerical integration program written in MatLab. The trapezoidal diffusion gradients were only applied in the read direction. It was found that the read gradients could not be ignored in our calculations. The diffusion effect of the read gradients was most pronounced for the Z echo. The gradients affecting the Z echo involved those between and including the second diffusion gradient and the Z echo read gradient (Fig. 1A). Since the time between the second and third diffusion gradients and the time between the read gradients were both on the order of 5 ms, inclusion of read gradients results in a larger fractional increase in the calculated b value for the Z echo, as compared to the P echo. In other words, for the Z echo, the read gradients add significantly to the attenuation from the diffusion gradients, and therefore cannot be ignored. The P echo attenuation, in contrast, arises primarily from the first and second diffusion gradients, since the time between

them is 32 ms whereas the time between the read gradients is only 1.6 ms. For example, under the experimental parameters of this paper (diffusion gradients = 38 G/cm(2 ms), read gradient = 7.9 G/cm(3.2 ms), dephasing portion of the read gradient = 8.8 G/cm(1.5 ms), diffusion time = 32 ms, T period = 11 ms, and TE_1 of 42 ms) the P echo b values with and without inclusion of the read gradients are 146,880 and 145,060 s/cm^2, respectively; the Z echo b values with and without inclusion of the read gradients are 42,860 and 32,581 s/cm^2, respectively.

The attenuation between the Z and Z2 echoes is expected to arise primarily from T_2 relaxation, since the b values of the two echoes are essentially the same (other than a small additional attenuation caused by the Z2 echo read gradient). Hence, T_2 can be obtained as

$$\ln\left(\frac{E(TE_Z)}{E(TE_{Z2})}\right) = \frac{TE_{Z2} - TE_Z}{T_2}, \tag{9}$$

where TE_Z and TE_{Z2} are the echo times for the Z and Z2 echoes, respectively. From the pulse sequence diagram in Fig. 1A, TE_Z is equal to TE_1 and, consequently, $TE_{Z2} = TE_1 + TE_2$. The accuracy and precision of a two-point measurement, of course, is limited and dependent on several factors. Therefore, to closely match the conditions under which the Z and Z2 echoes were collected, the same echo times were chosen in the control experiment.

3. Methods

All experiments were carried out on 400 MHz Bruker Avance scanner using the SMART P sequence described above. To calibrate the flip angle θ of the first RF pulse, the diffusion gradients were initially turned off and the angle varied until the P and Z echo intensities were equal. To obtain control ADC and T_2 measurements, a PGSE and double-spin–echo were used, respectively. To demonstrate the feasibility of the pulse sequence, two samples were used. The first sample (sample A) was a 5 mm o.d. NMR tube filled with 1 mM Gd-DTPA doped distilled water. The second sample (sample B) was a 5 mm o.d. NMR tube containing four sealed 1 mm o.d. capillaries immersed in 2% agarose prepared with distilled H_2O. Each capillary contained a mixture of D_2O (Cambridge Isotopes) and 1 mM Gd-DTPA doped H_2O of varying volume fractions (100% H_2O, 50% H_2O:50% D_2O, 30% H_2O:70% D_2O, and 10% H_2O:90% D_2O). In this manner it is ensured that each capillary differs in both T_2 and ADC. Heavy water is more viscous thus having a smaller ADC ($ADC_{D_2O,\,25^\circ C} = 1.87 \times 10^{-5}$ cm^2/s versus $ADC_{H_2O,\,25^\circ C} = 2.29 \times 10^{-5}$ cm^2/s [16]). Conversely, T_2 is prolonged with increasing D_2O fraction due to the deuteron's much smaller magnetic moment ($\gamma(^1H)/\gamma(^2H) = 6.5$) and, to a lesser extent, the lower concentration of Gd-DTPA.

Sample A was used to measure the ADC of water as well as to plot the echo amplitude dependence of the P, Z, and Z2 echoes on the flip angle of the first RF pulse in the absence of diffusion gradients. The parameters of sample A (1 mM Gd-DTPA doped H_2O) for the SMART P sequence were: $\theta = 67^\circ$, $T/TE_1/TE_2 = 11/42/50$ ms, $TR = 1000$ ms, slice thickness = 1 mm, FOV = 0.6 cm, matrix size = 64×64, number of acquisitions = 4, temperature = 22 ± 1 °C, diffusion gradient duration = 2 ms, diffusion time = 32 ms, receiver bandwidth = 20 kHz. $TE_Z = TE_1 = 42$ ms, and $TE_{Z2} = TE_1 + TE_2 = 92$ ms. A phase-cycling scheme was implemented with the transmit and receive phase in the four cycles set as follows: $\varphi_\theta(x, y, -x, -y)$, $\varphi^P_{rec}(-x, -y, x, y)$, $\varphi^Z_{rec}(-x, -x, -x, -x)$, and $\varphi^{Z2}_{rec}(x, x, x, x)$, where φ_θ is the phase of the initial θ RF pulse, and φ_{rec} is the receiver phase for each P, Z, and Z2 echo. The phase of the $\pi/2$ and π pulses are fixed at x and y, respectively. Slice-selective *sinc* pulses (three side lobes) of 1 ms duration were used. The diffusion gradients, G_d, were applied along the read axis and varied from 19 to 38 G/cm in steps of 4.75 G/cm. The crusher gradients were set at 9.5 G/cm and 1 ms duration.

The experimental parameters for the control PGSE ADC measurement of sample A were: diffusion time = 32 ms, diffusion gradient duration = 2 ms, $TE = 42$ ms, $TR = 1000$ ms, slice thickness = 1 mm, FOV = 0.6 cm, matrix size = 64×64, number of acquisitions = 1, temperature = 22 ± 1 °C, and receiver bandwidth = 20 kHz. Diffusion gradients were applied along the read axis and varied from 9.5 to 38 G/cm in steps of 9.5 G/cm. The parameters for the control double-spin–echo T_2 experiment were: $TE_1 = 42$ ms, $TE_2 = 92$ ms, $TR = 1000$ ms, slice thickness = 1 mm, FOV = 0.6 cm, matrix size = 64×64, number of acquisitions = 1, temperature = 22 ± 1 °C, and receiver bandwidth = 25 kHz. The same slice-selective *sinc* pulses defined above were used for the control experiments.

The parameters for sample B for both the control and SMART P experiments were the same as the first, except that $TR = 10$ s and slice thickness = 2 mm to improve SNR. When running the SMART P sequence, the flip angle of the θ RF pulse was 57.8° and the diffusion gradients were set to 38 G/cm.

4. Results and discussion

To verify that the P, Z, and Z2 echoes were in actuality arising from the predicted coherence transfer pathways, the echo intensity dependence on the first θ RF flip angle was measured for sample A (1 mM Gd-DTPA doped H_2O) (Fig. 2). The P, Z, and Z2 absolute signal intensities were normalized to their respective maximum values to compare only the effects of variation in flip angle. The plot indicates $\sin\theta$ and $\cos\theta$ flip angle dependence for the P and Z/Z2 echoes, respectively, as

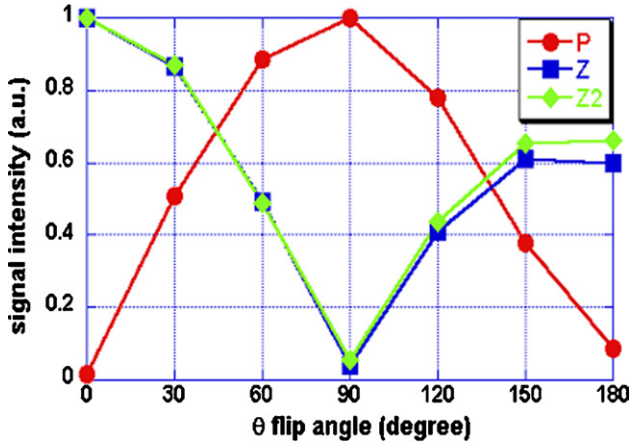

Fig. 2. P, Z, Z2 θ flip angle dependence with sample A. The intensities of the P, Z, and Z2 echoes depend on the flip angle of the θ RF pulse. The P, Z, and Z2 signal intensities have been normalized to their respective maximum values. Note the $\sin\theta$ and $\cos\theta$ dependence for the P and Z/Z2 echoes, as expected.

predicted from Eqs. (4) to (6). The deviation at higher flip angles is due to the well-known imperfections of large-angle slice-selective *sinc* pulses which can, of course, be remedied using adiabatic pulses, for example.

It should be mentioned at this point that the MMME method proposed by Song and Tang required no phase cycling of any kind. The SMART P sequence, however, required a four-step phase cycling scheme. The causes for the contamination of the P, Z, and Z2 echoes without phase cycling are not fully understood at this stage. However, there is evidence that off-resonance effects due to spatial selectivity of the RF pulses causes mixing between the coherence pathways. Song and Tang [3] demonstrated experimentally that off-resonance effects cause the maximum of the echoes to shift from the center of the readout window. The P, Z, and Z2 echoes may interfere with each other, requiring phase cycling to separate the signals. Further work is required to validate this theory.

Fig. 3 shows the ADC and T_2 maps for sample A (1 mM Gd-DTPA doped H_2O) created from the SMART P sequence. ADC and T_2 values as measured with SMART P are listed in Table 1 along with values obtained by conventional PGSE and double-spin–echo (DSE) methods. In the SMART P experiments, ADC and T_2 values were also calculated when the diffusion gradient strengths, diffusion time, and echo time separating the Z and Z2 echoes were all independently varied (data not shown). The values did not differ significantly from those in Table 1 thus suggesting that ADC and T_2 measurements in the SMART P sequence are uncoupled.

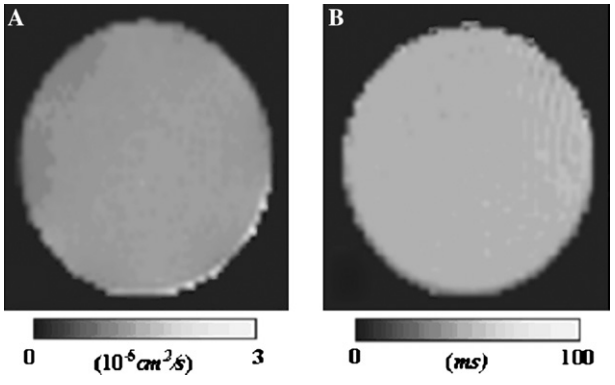

Fig. 3. SMART P maps for sample A: (A) ADC; (B) T_2.

Table 1
T_2 and ADC values of sample A (1 mM Gd-DTPA doped distilled H_2O) measured with various methods (DSE, PGSE, and SMART P)

Measurement	DSE	PGSE	SMART P
T_2 (ms)	85.6 ± 1.6	n/a	82.5 ± 1.1
ADC (10^{-5} cm^2/s)	n/a	2.19 ± 0.02	2.11 ± 0.06

The ROIs used were polygons with an area of at least 625 pixels and values listed were averages of at least five experiments.

Fig. 4A shows a diagram of the multi-compartment sample B, along with ADC and T_2 maps computed from the SMART P sequence (Figs. 4B and C). A typical set of P, Z, and Z2 images acquired with sample B ($G_d = 38$ G/cm) is shown in Figs. 5A–C. The calculated ADC and T_2 values from the SMART P and conventional PGSE and DSE methods are listed in Table 2.

The ADC and T_2 values calculated from the SMART P sequence show good agreement with the control values for both samples. It is noted that in the multi-compartment sample the standard deviation increased with

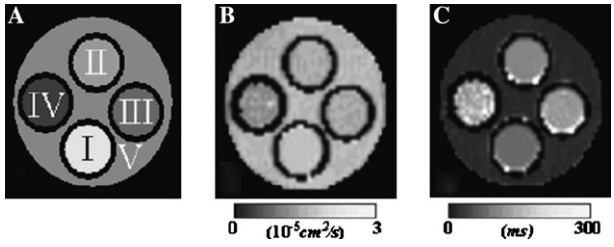

Fig. 4. (A) Diagram for sample B. All H_2O doped with 1 mM Gd-DTPA except for Region V, which was prepared with distilled H_2O. Region I: 100% H_2O. Region II: 50% H_2O:50% D_2O. Region III: 30% H_2O:70% D_2O. Region IV: 10% H_2O:90% D_2O. Region V: 2% agarose in H_2O. SMART P maps for sample B; (B) ADC; (C) T_2.

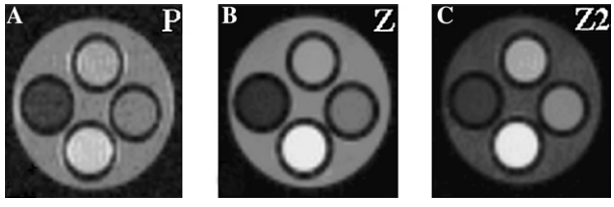

Fig. 5. Typical P (A), Z (B), and Z2 (C) images with the SMART P sequence.

Table 2
T_2 and ADC measurements of sample B (Fig. 4A) with various methods (DSE, PGSE, and SMART P)

Method	Region I (100% H_2O)	Region II (50% H_2O:50% D_2O)	Region III (30% H_2O:70% D_2O)	Region IV (10% H_2O:90% D_2O)	Region V (2% agarose)
DSE T_2 (ms)	98.4 ± 1.2	126.1 ± 4.3	145.4 ± 7.4	214.4 ± 35.0	40.9 ± 0.3
SMART P T_2 (ms)	106.0 ± 1.1	135.9 ± 1.8	154.1 ± 1.3	219.0 ± 22.4	43.0 ± 0.9
PGSE ADC (10^{-5} cm^2/s)	2.24 ± 0.02	2.02 ± 0.02	1.92 ± 0.02	1.77 ± 0.06	2.12 ± 0.02
SMART P ADC (10^{-5} cm^2/s)	2.25 ± 0.01	1.99 ± 0.02	1.93 ± 0.02	1.86 ± 0.07	2.12 ± 0.03

All H_2O doped with 1 mM Gd-DTPA. The ROIs used were polygons with an area of at least 20 pixels and values listed were averages of at least five experiments.

increasing D_2O volume fraction, caused by lower proton density and thus lower SNR. Instead of relying on two echoes for the calculation of T_2, it is, of course, possible to acquire a train of Z echoes, which should improve the precision of the derived T_2. In addition, the shorter inter-echo spacing time would reduce the effects of diffusion attenuation from field inhomogeneities and imaging gradients.

As mentioned earlier, an alternate version of the SMART sequence makes use of the coherence order -1 after the initial θ RF pulse to form the N echo, which would appear a period T (see Fig. 1A) after the Z echo. Currently, the minimum T period is 11 ms, which is limited by the TE_1 of the SMART P sequence to 42 ms, once the imaging gradients are taken into account. Therefore, the pulse sequence is limited to the measurement of relatively long T_2s ($\geqslant$40 ms). However, in the SMART N sequence, since the N echo appears after the Z echo, TE_1 would only be limited by the imaging gradients and RF pulses, so the minimum T_2 measurable would be on the order of 20 ms or longer.

Clearly, by combining ADC and T_2 measurements into one sequence, experimental scan time should be reduced as compared to running separate measurements. However, the scan times for the SMART P as compared with the total scan time of both the DSE and PGSE sequences are actually longer, when the number of different b value acquisitions is taken into account. The SMART P only acquires two different b values, while the control PGSE takes four. As it is the need to run separate experiments at each b value that causes long scan times, the SMART P method will begin to reduce scan time substantially when multiple b values are obtained, since it can acquire them simultaneously. It is clear that this could only be achieved by expanding the number of coherence pathways, which, in turn, requires additional RF pulses. There are many possible implementations of the SMART imaging method, ranging from using a greater number of RF pulses to generate a series of echoes, as discussed above, to using stimulated echoes, as opposed to the spin echoes in this paper, as the imaging sequence. Such extensions of the SMART method are beyond the scope of the present paper, which merely intended to demonstrate feasibility.

In conclusion, the feasibility of the MMME method for combined spatially localized measurement of ADC and T_2 has been demonstrated with the SMART P sequence. Conclusive evidence has further been provided on the basis of the flip angle dependence of the P, Z, and Z2 echoes that these signals do indeed arise from the predicted coherence pathways. The calculated ADC and T_2 values from the SMART P sequence are found to be in good agreement with those derived from conventional PGSE and DSE methods. Finally, the proposed approach offers multiple possible implementations which will be investigated in future work.

References

[1] E.L. Hahn, Spin echoes, Phys. Rev. 80 (1950) 580–594.
[2] E.O. Stejskal, J.E. Tanner, Spin diffusion measurements: spin echoes in the presence of time-dependent field gradient, J. Chem. Phys. 42 (1965) 288–292.
[3] Y.-Q. Song, X. Tang, A one-shot method for measurement of diffusion, J. Magn. Reson. 170 (2004) 136–148.
[4] C.J. Counsell, PREVIEW: a new ultrafast imaging sequence requiring minimal gradient switching, Magn. Reson. Imag. 11 (1993) 603.
[5] O. Heid, M. Deimling, W. Huk, QUEST—a quick echo split NMR Imaging technique, Magn. Reson. Med. 29 (1993) 280.
[6] P.P. Mitra, P.N. Sen, L.M. Schwartz, P. Le Doussal, Diffusion propagator as a probe of the structure of porous media, Phys. Rev. Lett. 68 (1992) 3555–3558.
[7] P.T. Callaghan, D. Mac Gowan, A. Coy, K.J. Packer, F.O. Zelay, Diffraction-like effects in NMR diffusion studies of fluids in porous solids, Nature 351 (1991).
[8] D.G. Cory, A.N. Garroway, Measurement of translational displacement probabilities by NMR, Magn. Reson. Med. 14 (1990) 435–444.
[9] K.R. Brownstein, C.E. Tarr, Importance of classical diffusion in NMR studies of water in biological cells, Phys. Rev. A 19 (1979) 2446.
[10] W.E. Kenyon, P.I. Day, C. Straley, J.F. Willemsen, A three-part study of NMR longitudinal relaxation properties of water-saturated sandstones, Soc. Petrol. Eng. Form. Eval. 3 (1988).
[11] F. D'Orazio, J.C. Tarczon, W.P. Halperin, et al., Application of nuclear magnetic resonance pore structure analysis to porous silica glass, J. Appl. Phys. 65 (1989).
[12] M.D. Huerlimann, L. Venkataramanan, Quantitative measurement of two-dimensional distribution functions of diffusion and relaxation in grossly inhomogeneous fields, J. Magn. Reson. 157 (2002) 31–42.

[13] P.T. Callaghan, S. Godefory, B.N. Ryland, Diffusion–relaxation correlation in simple pore structures, J. Magn. Reson. 162 (2003) 320–327.
[14] B. Manz, Combined relaxation and displacement experiment: a fast method to acquire T2, diffusion and velocity maps, J. Magn. Reson. 169 (2004) 60–67.
[15] D. van Dusschoten, C.T. Moonen, P.A. de Jager, H. Van As, Unraveling diffusion constants in biological tissue by combining Carr–Purcell–Meiboom–Gill imaging and pulsed field gradient NMR, Magn. Reson. Med. 36 (1996) 907–913.
[16] R. Mills, Self-diffusion in normal and heavy water in the range of 1–45 o, J. Phys. Chem. 77 (1973) 685–688.